

Damping LFOs: Grid Following with Power Oscillation Damping vs. Grid Forming vs. PSS

Tamojit Chakraborty
Member, IEEE
Siemens Energy
tamojit91@gmail.com

Anamitra Pal
Senior Member, IEEE
Arizona State University
Anamitra.Pal@asu.edu

Sam Maleki
Member, IEEE
RMS Energy Co. LLC
sam.maaleki@gmail.com

Abstract—Low-frequency oscillations (LFOs) present a significant challenge to the stability and reliability of power systems, especially in grids with a high penetration of renewable energy sources. Traditional grid-following (GFL) inverters have proven less effective in damping such oscillations. This paper presents a GFL-power plant controller with an auxiliary power oscillation damping control for damping LFOs. This approach is compared with a traditional power system stabilizer (PSS) for a two-area power system. Next, the research is extended by deploying grid-forming (GFM) controls, which by actively controlling the voltage and frequency dynamics emulate the behavior of traditional synchronous generators. The paper analyzes two GFM control strategies: virtual synchronous machine (VSM) and droop control, and demonstrates their effectiveness in damping LFOs in the test system. The simulation results reveal that the performance of the proposed GFM-VSM rivals that of the PSS and is better than the GFL-power oscillation damper.

Index Terms—Grid following, Grid forming control, Low frequency oscillation, Power oscillation damping, Stability

I. INTRODUCTION

The increasing adoption of converter interfaced generation (CIG) by displacing conventional synchronous machines (SMs) has reduced the system's inherent physical inertia and short circuit strength. Declining inertia negatively impacts system stability with electromechanical oscillations, typically in the range of 0.2 Hz to 2 Hz, often being affected by the penetration of CIGs [1]. A reduction in the damping of these oscillatory modes lowers the systems's stability margins resulting in sustained oscillations following an angle disturbance, heightening risks of unstable operating conditions. The risks vary based on grid conditions and the placement and control strategies of the CIGs [2].

The process of damping low-frequency oscillations (LFOs) relates to small-signal stability, which refers to the ability of a network to maintain synchronization when subjected to minor disturbances. The small-signal stability concerns stem from inadequate damping torque in SMs. Traditionally, power system stabilizers (PSSs) have been used to damp LFOs [3]. The primary function of a PSS is to enhance the damping of generator rotor oscillations by regulating the excitation system through an external control variable input. Typically, PSS consist of a gain block, a washout filter, and phase compensation blocks to correct for the phase lag of the excitation system.

The displacement of SMs and the rise of CIGs have intensified rotor oscillations and their impact on system frequency [4]. To address these issues, power oscillation damping (POD) controllers whose structures are similar to PSSs, have been used as auxiliary controls of flexible AC transmission system (FACTS) and high-voltage DC (HVDC) systems [5], [6]. These devices dampen oscillations by injecting active power (POD-P) or reactive power (POD-Q) to regulate voltage at the point of interconnection.

POD controllers used in conjunction with power plant controllers (PPCs) in grid-following (GFL) inverters have been proposed for actively adjusting the inverter's output to counteract destabilizing oscillatory modes [7], [8]. A step forward is using grid forming (GFM) inverters [9] that offer rapid response to disturbances in the network by utilizing a synchronization loop that emulates the behavior of a SM [10]–[12]. For example, [13] presents a centralized controller to damp LFOs utilizing virtual synchronous generators.

Considering the status of present literature, this paper develops two new user-defined control models for damping LFOs in renewable-rich power systems and compares their performance for a multi-area test system. Our main contributions are:

- 1) *Auxiliary POD function in PPC model*: A GFL-POD controller function is developed on a PPC user-defined model (UDM) that has two choices to damp LFOs: using active power, frequency (POD-P) or reactive power, bus voltage (POD-Q) signals. The structure of the POD consists of a deadband, a low pass filter, a washout block, and a lead-lag block for phase compensation.
- 2) *GFM controller Model*: A GFM UDM is developed in PSS/E with four control layers: the outer layer emulates a synchronous generator's swing dynamics with adjustable inertia and damping while a virtual excitation control provides a voltage reference. A current controller that utilizes voltage and frequency droop to generate current commands which forms a voltage source behind an internal impedance.
- 3) *Comparison of Strategies*: The developed POD and GFM UDMs are compared against different GFM strategies proposed in [14] and a traditional PSS for a two-area benchmark system. Detailed eigenvalue analysis results and damping ratios are presented for each strategy.

II. MODELING AND IMPLEMENTATION OF CONTROLLER STRATEGIES

A. Power Oscillation Damping Controller Architecture

This section presents the design and implementation of the GFL-POD controller. Since the WECC generic REPCA model lacks POD functionality, a custom PPC model was developed in PSS/E. This PPC model offers several features [15], including voltage, power factor, reactive power, and frequency control, in addition to the POD functionality. Note that the proposed POD control shares a structural resemblance to a conventional PSS. For POD-P, either active power measurement at a branch or bus frequency can be used, while for POD-Q, either reactive power measurement at a branch or bus voltage serves as the input. Fig. 1 shows the block diagram of the POD controller. The dynamics of this controller are outlined below:

$$\frac{ds_0}{dt} = (1/T_f) * [V_{inp} - s_0] \quad (1)$$

$$\frac{ds_1}{dt} = (1/T_w) * [K_w * s_0/T_w - s_1] \quad (2)$$

The first block labeled s_0 is a low-pass filter that filters high-frequency signals, allowing only low-frequency components to pass through. It stabilizes the input signal (V_{inp}) by reducing noise and rapid fluctuations. The washout block (s_1) filters out steady-state or low-frequency components, allowing only oscillatory (dynamic) components of the input signal to pass. This ensures that oscillations are damped effectively without impacting the steady-state power or voltage levels. The two lead-lag compensators (s_2 and s_3) are used to phase-shift the signal appropriately to counteract oscillations. The lead part introduces phase advance, which helps to counteract phase lags in the system, while the lag part stabilizes the response. These blocks adjust the phase and magnitude of the signal to maximize the damping of oscillations at specific frequencies. Finally, the limiters ensure that the output remains within a predefined range, preventing excessively high or low control signals that could destabilize the system. In summary, the POD controller uses a lag block for signal smoothing, a washout block to isolate oscillatory components, and lead-lag blocks to provide phase correction, allowing it to effectively dampen power oscillations in the system.

B. Grid Forming Model Control Architecture

The core control structure of a GFM comprises an outer voltage controller and an inner current controller. The outer control consists of active power-frequency (P-F) and reactive power-voltage (Q-V) control. In our proposed GFM model, the outer-level P controller has an integrator and a first-order time constant. They mimic the dynamics of the swing equation of a SM and generate a frequency reference. The virtual excitation control generates a voltage reference using a proportional-integral (PI) controller. An inner current controller uses voltage and frequency droop to generate active and reactive current commands that are used to form a voltage source behind an internal impedance. Finally, a phase-locked loop (PLL) is

used to convert the machine's rotational reference frame to the network's frame of reference. A PLL can still be utilized in a GFM, as this model supports rapid current injection (at a sub-transient timescale) by maintaining its internal voltage magnitude and angle. This conclusion is consistent with the findings in [16].

The GFM controller was developed as a custom UDM in PSS/E, utilizing FORTRAN code for implementation. PSS/E uses the modified Forward Euler method for numerical integration, updating state variables and their derivatives at each time step. In this model, current limits are implemented as per WECC MVS guidelines [17]. Equations (3) and (4) represent the droop controller dynamics through simple first-order lag blocks (see Fig. 2), while current controller dynamics shown in Fig. 3 are outlined in (5) and (6), respectively. The voltage source interface of the GFM model is shown in Fig. 4.

$$\frac{ds_{14}}{dt} = (1/T_{vdrp}) * [(I_d * K_{vd} + I_q * K_{vq}) - s_{14}] \quad (3)$$

$$\frac{ds_{15}}{dt} = (1/T_{fdrp}) * [(I_d * K_{fd} + I_q * K_{fq}) - s_{15}] \quad (4)$$

$$\frac{ds_{11}}{dt} = K_{in} * [W_{pr} - F_d - s_{11}] \quad (5)$$

$$\frac{ds_{13}}{dt} = K_{iv} * [V_{pr} - V_d - s_{13}] \quad (6)$$

C. Other Grid Forming Control Strategies

The WECC REGFMA1 [14] model is employed to benchmark system performance against the proposed GFM and POD models. REGFMA1 incorporates P-F and Q-V droop controls, with active and reactive power limiting controls, and includes fault current limiting controls. The P-F control block participates in frequency regulation by adjusting the P output of the resource in response to grid frequency changes, while the Q-V control block aids in voltage regulation.

III. STABILITY ANALYSIS

A. Two-Area System

The control schemes presented in the previous section are employed to study the damping of LFOs in Kundur's two-area benchmark system. The system consists of two synchronous generators SG1 and SG2, connected through their corresponding step-up transformers, and interconnected through two parallel lines between buses 2 and 3. A CIG device is also connected at Bus 2 through a step-up transformer. The SG1 and SG2 have a generation of 925 and 1300 MW, respectively, serving their local loads of 1000 and 1300 MW, respectively. The CIG device whose dynamic characteristics are varied to study different control strategies has a rating of 75 MW. It is considered that the impedance across the tie line connecting Buses 2 and 3 is variable. The loads have been modeled as ZI loads by assuming constant current for P and constant impedance for Q. SG1 and SG2 are modeled using GENROU mode with ESST4B excitation system and TGOV1 governor model. To evaluate the system performance with PSS, the CIG

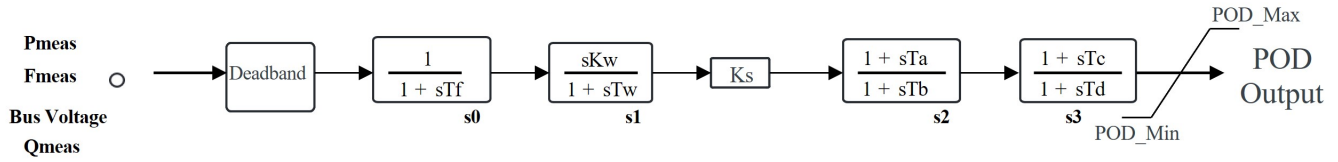


Fig. 1. Proposed GFL-POD Controller

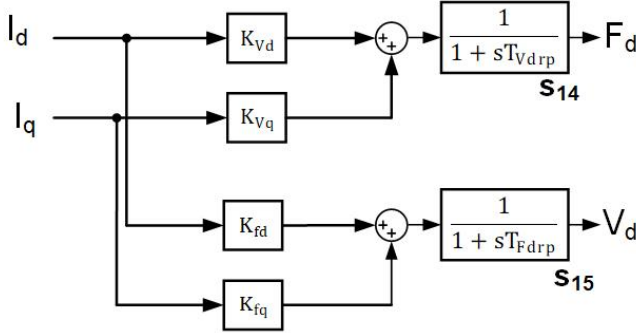


Fig. 2. Droop Controller

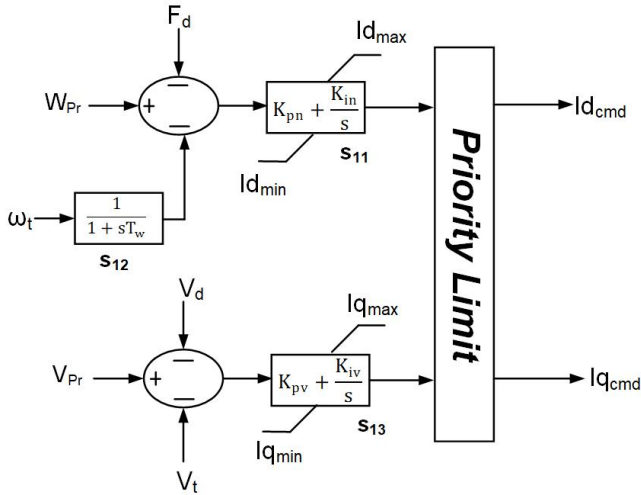


Fig. 3. Current Controller

device is disconnected and the SG1 generates 1000 MW. The PSS model used in this study is the PSS2B.

The electrical model of the CIG with the POD used in this study consists of the generator converter model REGCA and electrical control model REECA and a user-defined PPC model in PSS/E. The variables VFlag and QFlag in the REECA model [18] are set to 1. The end-user has a choice through a flag to activate the POD in either the P control or the Q control mode. For POD-P, the user can either choose the frequency deviation at a bus or active power flow in a branch to modulate the direct axis current of the resource. A similar concept applies to the POD-Q logic where the end user can choose either a bus voltage or reactive power flow across a branch to modulate the quadrature axis current.

For the GFM control strategies, the UDM described in the previous section is utilized. There are two possible model vari-

ants within the UDM: (a) virtual synchronous machine (VSM) combined with droop control, and (b) droop control alone. The VSM offers natural damping to the system, mimicking the dynamics of a SM. Similarly, the droop control-based GFM responds quickly to disturbances within the system. The ability of both the model variants were investigated in this study. Lastly, the WECC REGFM model with typical parameters [14] is employed as an additional GFM control strategy.

B. Simulation Set-up

Several simulations have been performed on the two-area test system to gain insights into the performance of the different controller strategies described in this paper. To induce LFOs in the system the tie line impedance across Bus 2 and Bus 3 is varied to make the system reach a marginally stable condition. Then, a 15ms solid three-phase-to-ground is applied at Bus 2. As can be seen in Fig. 6, the tie line shows LFOs.

Next, a dual input PSS is applied at Bus 2 that uses generator active power and rotor speed deviation as inputs to enhance the damping of LFOs and improve system stability. By processing both inputs, it captures dynamic fluctuations in power flow and system frequency deviations, which indicate disturbances or imbalances. Each input passes through washout filters to remove steady-state components and lead-lag compensators to align the PSS's corrective actions with oscillation frequencies. The combined output is applied to the generator's excitation system to counteract oscillations, providing robust damping and improved overall system stability.

For the GFL case with POD as well as the GFM case, a similar disturbance is introduced into the system, and each control strategy tries to mitigate the resulting oscillations through its dynamic response. In the GFL case, the POD-P and POD-Q controllers activate upon detecting LFOs, while the GFM units address system disturbances by closely regulating voltage magnitude and angle at their terminals.

C. Eigenvalue Analysis

Fig. 7 shows the eigenvalues for different configurations on the complex plane, with the X-axis representing the real part (damping) and the Y-axis representing the imaginary part (oscillation frequency). Negative real values suggest that oscillations decay over time, enhancing stability. Eigenvalues closer to the origin indicate lower frequencies and slower oscillations, while those farther away may indicate more dynamic responses. Table I shows the eigenvalues for each control strategy. The eigenvalues are obtained by performing Prony Analysis using PSS/E built-in program PSSPLT.

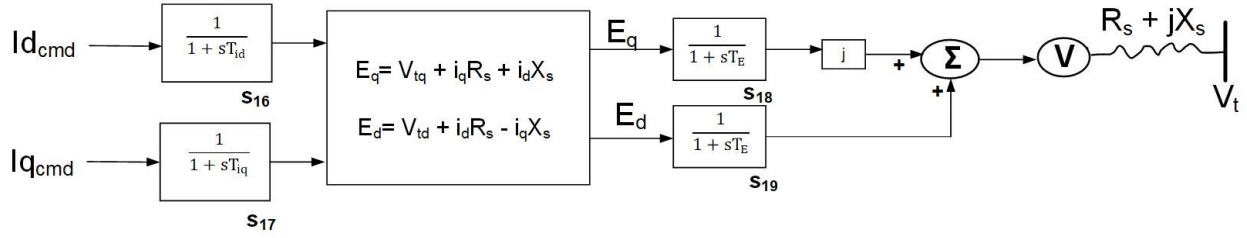


Fig. 4. VSC Interface for the Proposed GFM

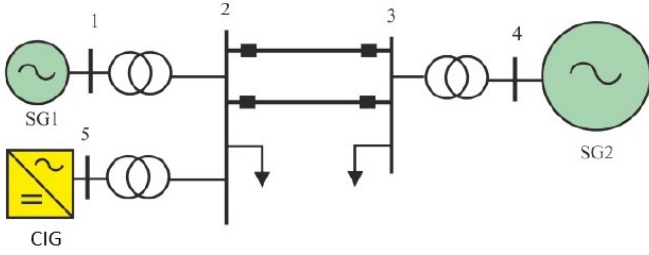


Fig. 5. Two-area System with CIG Device

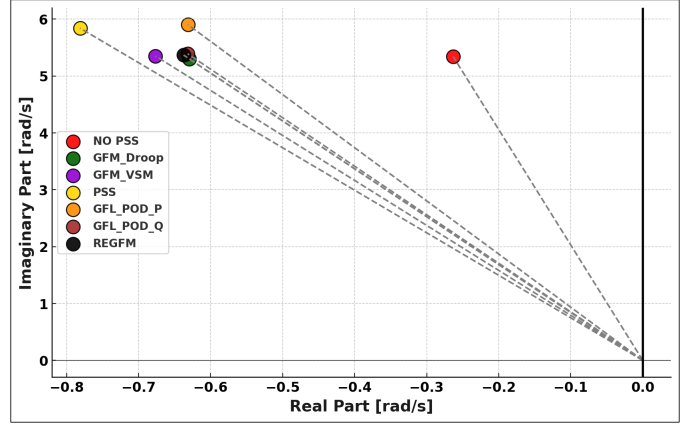


Fig. 7. Eigenvalues for Different Scenarios

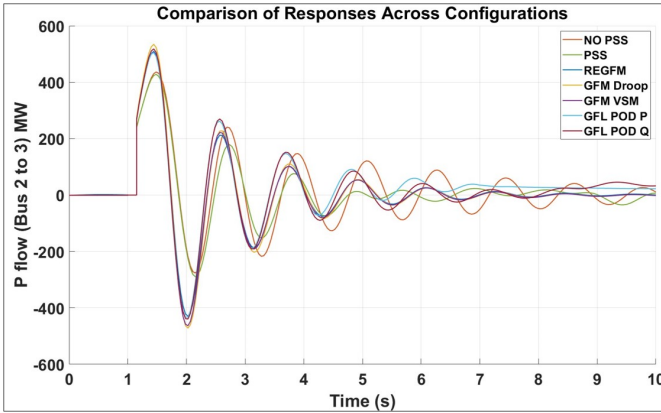


Fig. 6. Active Power Flow from Bus 2 to 3 when Tie Line Impedance Changes

Overall Comparison: The eigenvalue comparison reveals that the PSS provides the highest damping effect overall, with the most negative real part, enabling oscillations to decay quickly and enhancing stability. The GFM-VSM also offers strong damping, though slightly less than the PSS, maintaining stability without significantly increasing oscillation frequency. The GFL equipped with POD-P provides moderate damping, better than NO PSS but less than PSS, GFM-VSM, GFM-Droop, REGFM, and POD-Q, with a relatively high frequency, suggesting a more dynamic response. In contrast, NO PSS has the lowest damping, as indicated by its least negative real part, which could lead to prolonged oscillations.

GFL-POD-P vs. GFL-POD-Q: The GFL with POD-P and POD-Q configurations show similar oscillation frequencies, as indicated by their close imaginary parts (5.90218 and 5.39, respectively, in Table I). However, they differ in damping effectiveness. The POD-P has a real part of -0.631503 and a damping ratio of 10.6%, providing moderate damping. In

contrast, the POD-Q has a slightly more negative real part (-0.631767) and a higher damping ratio of 11.6%, suggesting that it will stabilize oscillations slightly faster than POD-P, making it marginally more effective in damping oscillations.

GFM-VSM vs. GFM-Droop: The GFM-VSM has a real part of -0.676476 and a damping ratio of 12.5%, indicating a strong damping effect and stable response. The GFM-Droop, with a real part of -0.629683 and a damping ratio of 11.8%, offers slightly less damping, meaning oscillations decay a bit slower than with the GFM-VSM. Its imaginary part (5.29911) is also slightly lower, indicating a slightly slower oscillatory response. Overall, GFM-VSM provides a stronger damping effect and faster stabilization compared to GFM-Droop.

Proposed GFM Control vs. Proposed GFL-POD-Q vs. REGFM [14]: The GFM-VSM provides stronger damping and faster stabilization than REGFM, with a higher damping ratio of 12.5% and more negative real parts for quicker oscillation decay. In contrast, the GFM-Droop and REGFM show similar performance, indicated by comparable damping ratios and eigenvalue real parts. Comparing the GFL against the GFM strategies, the GFM-VSM provides stronger damping and faster stabilization than GFL with POD-Q, though both show similar oscillation frequencies and dynamic behavior. Overall, the proposed GFM-VSM outperforms the others in terms of damping effectiveness and stability.

D. Dynamic Response to Load Change

This section analyzes the dynamic response of the two-area power system when subjected to a 150 MW load reduction

TABLE I
RANKED EIGENVALUES AND DAMPING RATIOS FOR DIFFERENT
CONTROL STRATEGIES

Strategies	Real	Imag	Damping Ratio
PSS	-0.781214	5.84032	13.3
GFM_VSM	-0.676476	5.34967	12.5
REGFM [14]	-0.637492	5.36776	11.8
GFM_Droop	-0.629683	5.29911	11.8
GFL_POD_Q	-0.631767	5.39000	11.6
GFL_POD_P	-0.631503	5.90218	10.6
NO PSS	-0.263220	5.34158	4.9

at Bus 2. Without any PSS, the sudden load decrease causes oscillations in the tie line leading to prolonged instability (see Fig. 8). With the GFM-VSM, the system's response improves substantially (rivaling that of PSS). Specifically, the GFM-VSM immediately counteracts the oscillations in the tie line by modulating its power output. This rapid response highlights the GFM-VSM's capacity to mimic the behavior of traditional SMs, making them a valuable asset for enhancing grid resilience, especially under sudden changes in load or generation. In summary, the results demonstrate that the proposed GFM-VSM with its machine-like dynamic performance, is well-suited for modern grids seeking enhanced stability and robust response for damping LFOs.

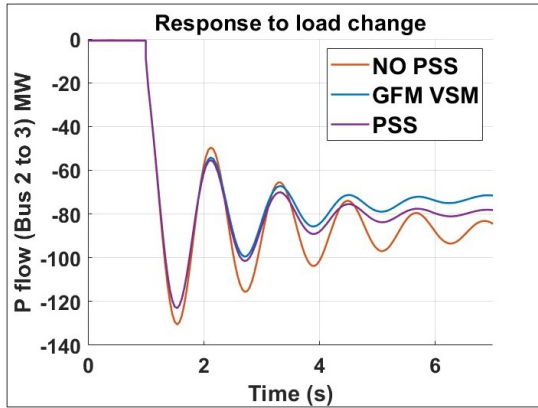


Fig. 8. Active Power Flow from Bus 2 to 3 when Load changes

IV. CONCLUSION

This paper examines the impact of LFOs on system stability and explores mitigation strategies amid the growing integration of CIGs and the retirement of traditional SMs. A GFL-POD controller is designed and implemented as an auxiliary function within a PPC, and a PSS/E UDM is developed to evaluate the controller's effectiveness in two modes: POD-P and POD-Q. Additionally, a GFM controller is developed to compare its functionality with the GFL-POD controls. The proposed GFM controller includes an outer loop that replicates SM swing dynamics, along with P-F and Q-V droop control. Both the GFL-POD and GFM controls are tested in a two-area test system, and a detailed small-signal stability analysis is conducted. The results demonstrate the effectiveness of GFM controls (particularly, proposed GFM-VSM) in damping LFOs

to a similar extent as a traditional PSS. This study provides valuable insights for a specific test system; future work will explore broader applicability in more complex networks.

REFERENCES

- [1] P. Tielens and D. Van Hertem, "The relevance of inertia in power systems," *Renewable and Sustainable Energy Reviews*, vol. 55, pp. 999–1009, 2016. [Online]. Available: <https://www.sciencedirect.com/science/article/pii/S136403211501268X>
- [2] S. Eftekharnajad, V. Vittal, G. T. Heydt, B. Keel, and J. Loehr, "Small signal stability assessment of power systems with increased penetration of photovoltaic generation: A case study," *IEEE Transactions on Sustainable Energy*, vol. 4, no. 4, pp. 960–967, 2013.
- [3] A. Pal, J. S. Thorp, S. S. Veda, and V. Centeno, "Applying a robust control technique to damp low frequency oscillations in the WECC," *International Journal of Electrical Power & Energy Systems*, vol. 44, no. 1, pp. 638–645, 2013. [Online]. Available: <https://www.sciencedirect.com/science/article/pii/S0142061512004589>
- [4] Y. Fan, S. Niu, M. Wang, Y. Wang, and C. Wang, "Low frequency oscillation analysis of power system with large-scale renewable energy access," in *2023 IEEE 2nd International Power Electronics and Application Symposium (PEAS)*, 2023, pp. 803–806.
- [5] D. Roop, T. Chakraborty, and S. Morello, "Selective power oscillation damping control system with damping ratio dynamic gain and method for the same," April 2023, US Patent US11637428B2. [Online]. Available: <https://patents.google.com/patent/US11637428B2/>
- [6] P. Gupta, A. Pal, and V. Vittal, "Coordinated wide-area control of multiple controllers in a power system embedded with HVDC lines," *IEEE Transactions on Power Systems*, vol. 36, no. 1, pp. 648–658, 2021.
- [7] Y. Zhao, K. M. Alshuaibi, X. Jia, C. Zhang, Y. Liu, D. Ramasubramanian, L. Zhu, and E. Farantatos, "Comparison of wide-area and local power oscillation damping control through inverter-based resources," in *2023 IEEE Power & Energy Society Innovative Smart Grid Technologies Conference (ISGT)*, 2023, pp. 1–5.
- [8] S. Alalwani, S. Isik, and S. Bhattacharya, "Inter-area oscillation damping controller for DFIG based wind power plants," in *2022 IEEE Energy Conversion Congress and Exposition (ECCE)*, 2022, pp. 1–6.
- [9] S. Maleki, T. Chakraborty, B. Yancey, A. K. Chen, and H. Trahan, "Utility-based grid forming inverters applications: Seamless transition and power oscillation damping," in *2022 IEEE/PES Transmission and Distribution Conference and Exposition (T&D)*, 2022, pp. 1–5.
- [10] J. L. Rodríguez-Amenedo and S. A. Gómez, "Damping low-frequency oscillations in power systems using grid-forming converters," *IEEE Access*, vol. 9, pp. 158 984–158 997, 2021.
- [11] J. C. Martínez, F. Gonzalez-Longatt, S. A. Gómez, and J. L. Rodríguez Amenedo, "Low-frequency oscillations damping with doubly-fed induction generators embodying grid-forming control with hardware-in-the-loop simulation," *International Journal of Electrical Power & Energy Systems*, vol. 157, p. 109896, 2024. [Online]. Available: <https://www.sciencedirect.com/science/article/pii/S0142061524001170>
- [12] L. Zhu, et al., "Power oscillation damping through grid forming inverters," EPRI, Tech. Rep., 2023.
- [13] J. Feng, F. Bai, M. Nadarajah, H. Ma, and A. Pradana, "Virtual inertia control for damping low-frequency oscillation in IBR-dominated networks," *IEEE Transactions on Industry Applications*, pp. 1–10, 2025.
- [14] W. Du, Q. H. Nguyen, S. Wang, J. Kim, Y. Liu, S. Zhu, F. K. Tuffner, and Z. Huang, "Positive-sequence modeling of droop-controlled grid-forming inverters for transient stability simulation of transmission systems," *IEEE Transactions on Power Delivery*, vol. 39, no. 3, pp. 1736–1748, 2024.
- [15] T. Chakraborty, S. Maleki, S. Mohan, K. Samarasekara, B. Yancey, Z. Qu, G. Alian, and H. Trahan, "Design, implementation, and application guidelines of master power plant controllers in dynamic analysis for grid code requirements," in *2023 IEEE Kansas Power and Energy Conference (KPEC)*, 2023, pp. 1–4.
- [16] N. Mohammed, H. Alhelou, and B. Bahrani, *Grid-Forming Power Inverters: Control and Applications*, 1st ed. Australia: CRC Press, 2023, publisher Copyright: © 2023, All rights reserved.
- [17] D. Ramasubramanian, "Implementation of current limit logic in REGCB and REGCC," EPRI Memo for WECC MVS, Tech. Rep., 2019.
- [18] T. Chakraborty and A. Pal, "Controller tuning of generic positive sequence solar PV models used in interconnection studies," in *2017 North American Power Symposium (NAPS)*, 2017, pp. 1–6.